Modeling Dye Assisted Photocoagulation of Age-Related Macular Degeneration

BEE 4530 – Computer Aided Engineering: Applications to Biomedical Systems

Lee Cadesky, Jun Hyuk Suh, Hongyi Tian

Contents

1.0 Executive Summary

Age-related macular degeneration (AMD) is major cause of blindness in Americans aged 50 years and up. In 2010, there were more than 2 million cases of AMD in the United States and the National Eye Institute projects that there will be nearly 5.5 million cases per year by 2050. The more detrimental form of AMD, the "wet" form, is caused by the development of new blood vessels within the macular region of the eye, a condition known as choroidal neovascularization (CNV). Several treatment modalities are available for AMD, however the most common is laser photocoagulation in which the abnormal blood vessels are coagulated using a high intensity laser as a heating source. While this treatment modality is effective, high temperatures within the deep eye tissue can cause unwanted collateral damage. Optimizing this thermal treatment thus amounts to minimizing the duration of treatment such that the abnormal blood vessels are destroyed but damage to other tissues is minimized. One possible extension was also explored in this study which is the injection of highly absorbent dye into the abnormal feeder vessel to improve the laser absorbance.

The model used in this study employs a 3D Cartesian geometry over which Pennes bioheat equation is solved for the temperature profile over a time scale of 1 second. The thermal damage is then analyzed by observing the temperature history in abnormal and healthy tissue with the goal of achieving a cumulative effective number of minutes at 43^{o}C greater than 80 minutes within the target tissue, the feeder vessel, while minimizing the thermal damage elsewhere. Results from the model suggest that after 1 second of laser application, temperatures in the feeder vessel rapidly rise to a maximum of 67^{o}C and temperatures in the retinal pigment epithelium (RPE) rise to 86^{o}C. In the hottest section of the feeder vessel, that section which is directly exposed to the center of the laser spot, the desired thermal damage is achieved within 0.55 s. The model was assessed for sensitivity to thermal properties as well as the absorbance coefficient, μ_a, in the feeder vessel and RPE sections. Results from this analysis suggested a change in temperature of less than 0.5% when these parameters were varied within the reasonable limits found in the literature. This suggests good applicability of the results to individual patients.

The use of dye to target and improve heat transfer is a novel improvement to the existing photocoagulation process. To assess the efficacy of such a modification, the absorbance coefficient was increased from 4610 m^{-1} to 9000 m^{-1} to simulate the effect of the dye. The results show very little variation in feeder vessel temperatures suggesting that dye assisted photocoagulation is not a large improvement from the current process. The effect of blood flow velocity was also assessed in this study. As expected, it was found that increasing blood flow velocity shifted the maximum temperature in the feeder vessel along the direction of flow and resulted in slightly lower maximum feeder vessel temperatures as the blood cools the feeder vessel by convection. The results of this study suggest that shorter treatment times may be useful in reducing collateral tissue damage, however a treatment time of 1 second is justified as a margin of safety to ensure complete destruction of the desired tissue.

1.1 Introduction

Age-related macular degeneration (AMD) is still the leading cause of blindness in people over 50 years of age in industrialized countries. About 8.7% of all blindness is caused by AMD, which has both 'wet' and 'dry' forms, with the dry form being more frequent but less detrimental to patients than the wet form. Wet form AMD is characterized by the development of abnormal, new blood vessels deep in the sensory retina, which may leak or bleed, leading to marked loss of central vision (WHO, 2007). The cause of wet form of AMD is called choroidal neovascularization (CNV). CNV attacks the sensory retina of the eye by affecting the macula and the fovea, the areas of the retina where acute central and color vision are governed. As CNV develops, immature vessels leak fluid, producing edema that distorts the retinal tissue, resulting in reduced visual acuity. Often, these newly formed vessels rupture and result in a copious discharge of blood. In more severe situations, the formation of CNV can lead to retinal detachment, which directly causes vision loss. There are numerous medical treatments for AMD-related CNV, including surgical removal, macular translocation, photo-dynamic therapy, various anti-angiogenic drugs, and laser photocoagulation (Zhu et al., 2008).

Of various treatment options, surgical translocation of the macula and submacular surgery can be performed only for selected patients. Even then, such surgery requires highly experienced vitreo-retinal surgeons and the results are not always favorable, due to its risk of damaging underlying retinal pigment epithelium (RPE) and the Bruch's membrane (Gass, 1994). Photodynamic therapy can also be offered to selected patients, but the long-term outcomes are not uniformly good. Moreover, while sequential intravitreal injections of anti-vascular endothelial growth factor agents can improve vision or stabilize visual loss in patients, this treatment is very expensive and time-consuming (WHO, 2007). The current research focus is to extend the traditional domain of the laser treatment, which were previously confined to the superficial layers associated with the retina, to laser photocoagulation in which laser energy must penetrate the overlying retinal tissues. Considering the other options, laser photocoagulation of the feeder vessels of the AMD-related CNV membrane is a compelling treatment modality and simulation is an effective means to better understand, and improve, its application.

The basic mechanism of laser photocoagulation is that by selectively photocoagulating the feeder vessel, which supplies blood to choriocapillaries, the blood pressure gradient within the choriocapillaries can be manipulated in such a way as to eliminate or reduce the hemodynamic force that drives blood through the CNV membrane. It is interesting that the use of indocyanine green (ICG) dye during the laser photocoagulation enhances the CNV feeder vessel coagulation process. The reason behind is that the peak emission wavelength of the diode laser (~805 nm) closely matches with the peak absorbance wavelength of ICG dye (~800 nm), thus improving laser energy absorption if the laser energy is applied when a concentrated dye bolus moves through the targeted feeder vessel.

The main focus in this simulation-based study is, with the use of COMSOL, to successfully model coagulation process of the feeder vessel and surrounding tissue sections in the eye with the goal of determining a laser heating regime that maximizes thermal damage to the feeder vessel, while minimizing unwanted damage to other tissue sections.

2.0 Problem statement

Though the use of laser-induced photocoagulation on feeder vessels is appealing, there is still a challenge in this modality. Direct and contiguous laser treatment of the entire subfoveal lesion damages the foveal and macular regions and is often associated with an immediate loss of central vision following the treatment. In order to overcome this challenge, the temperature distribution in the vicinity of feeder vessel during the photocoagulation procedure is modeled in COMSOL, and the heat transfer within the region was optimized such a way that minimizes the thermal damage to surrounding tissue. Detailed discussion of thermal damage calculations and criteria can be found in Appendix A.

2.1 Design objectives

The main focus of this study is the model the temperature rise in the feeder vessel and surrounding tissue during laser photocoagulation. The main objectives are outlined below and establish the criteria for effective destruction of the target tissue as well as research extensions.

1. Obtain a temperature profile in the vicinity of the feeder vessel
2. Determine the optimal laser duration for the procedure to ensure complete removal of the feeder vessel (CEM43^{o}C > 80) while minimizing thermal damage to nearby tissues
3. Explore the effect of laser application duration, dye assisted photocoagulation, and blood flow velocity on the tissue temperature profile

2.2 Model assumptions

To simplify the modeling of otherwise complex and anisotropic tissue, numerous assumptions had to be considered in the development of the computational model. While these assumptions reduce the physical accuracy of the solution, they are essential to facilitating the development of a model and are in concert with assumptions generally used in the development of computational models of biological tissue.

- Curvature of the eye is neglected for the small cross section of interest
- The feeder vessel is modeled as a cylinder of constant diameter
- The feeder vessel wall is assumed to be thin, so heat transfer through the solid wall may be neglected
- Metabolic heat generation is neglected
- All tissue properties are considered constant and isotropic
- The dye bolus is transferred through the feeder vessel only and there is no mass transfer through the walls of the feeder vessel over the time interval of interest. Mass diffusion of the dye is negligible over the time interval of interest
- Blood flow in the feeder vessel is modeled as plug flow with constant viscosity over the temperature range observed
- Laser fluence is assumed to be steady state, this is validated by calculations presented in Appendix A
- Laser light diffusion is assumed to be anisotropic within the vitreous section and isotropic in all other tissue sections. This is to account for the relatively small diffusion that occurs within the vitreous section. To better model laser heating in the eye, the laser application

is assumed to take place directly at the retina rather than the vitreous section. Loss of laser energy is accounted for by attenuating the laser intensity at the retina by a factor of 5% as explained in Appendix A.

3.0 Results

The model was solved for laser fluence, temperature, and velocity field in the feeder vessel. These results are presented individually in the following sections.

3.1 Velocity in Feeder Vessel

The velocity field in the feeder vessel was evaluated at steady state conditions for an initial blood velocity of 0.02 m/s. The results show a parabolic flow profile as would be expected for laminar, pipe flow. Considering the thinness of the feeder vessel and the small effect the velocity field has on the feeder vessel temperature, subsequent studies of the temperature profile were done under the assumption of plug flow at a constant velocity within the feeder vessel. This was done to reduce the computation time of the model and results compared well with solutions obtained using the full velocity field.

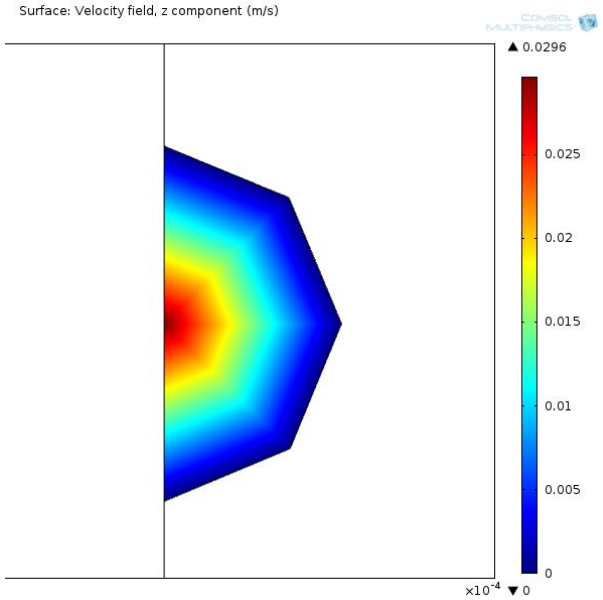

Figure 1: Velocity field (z-component) in feeder vessel. Scale represents z-component velocity in m/s. The velocity field is axisymmetric with a parabolic profile as would be expected for laminar flow. This field was not introduced into the temperature studies as the effect of the flow profile on temperature was not significant.

3.2 Laser Fluence and Temperature

The temperature after 1 second of laser application is shown in Figure 2 and Figure 3 below. The computation was performed for from 0 to 1 second of laser application with a time step of 0.05 s, using COMSOL's default solver.

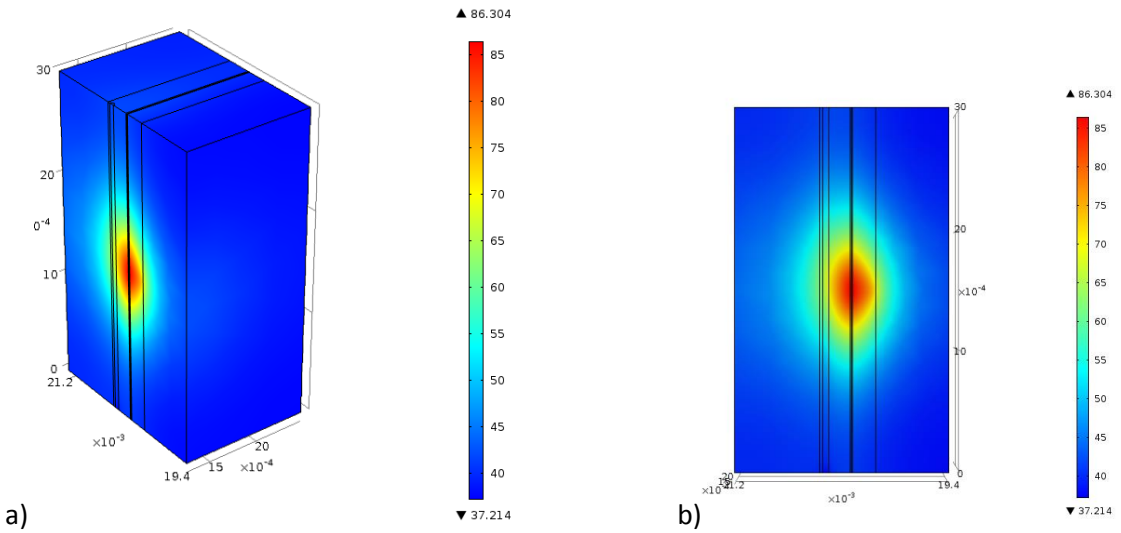

Figure 2: Temperature profile after 1 second of laser heating a) isometric view; b) surface of intense laser heating; c) Full geometry, isometric view; d) Top view; All temperatures in ^{o}C, all dimensions in m. Intense heating is observed near the laser application and radiates outward. The temperature gradient decays to zero at the far ends of the model, justifying a semi-infinite boundary condition.

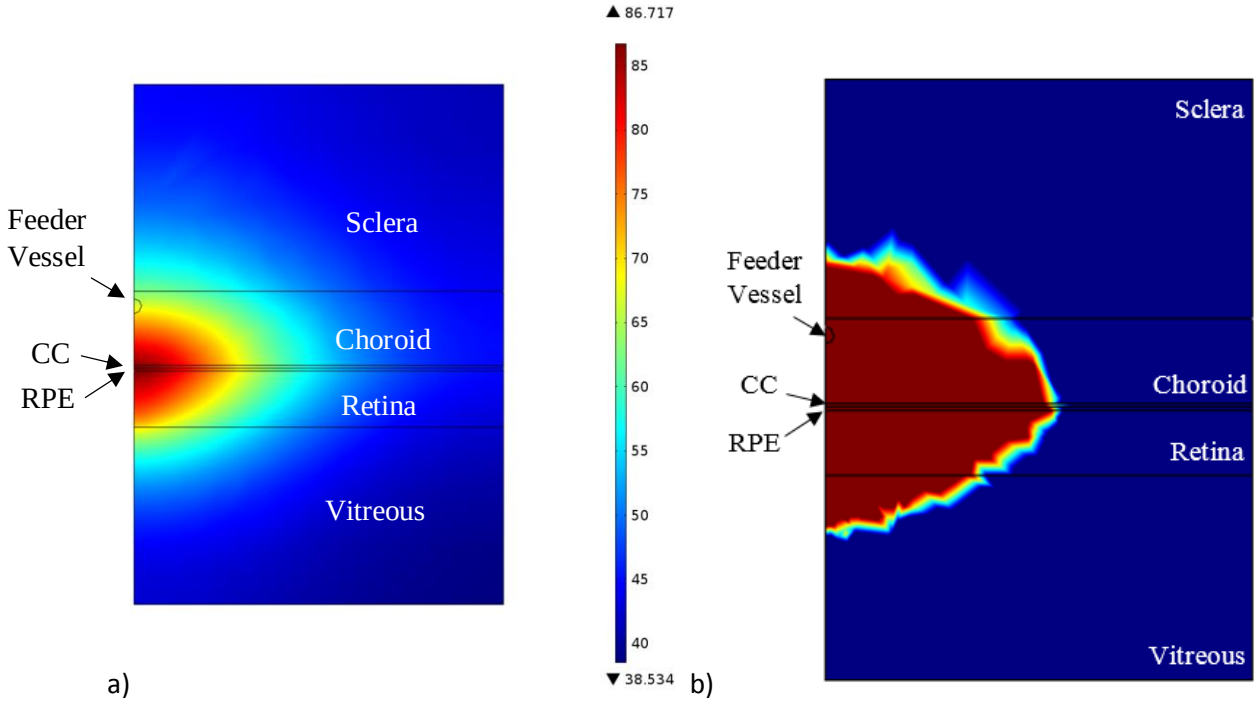

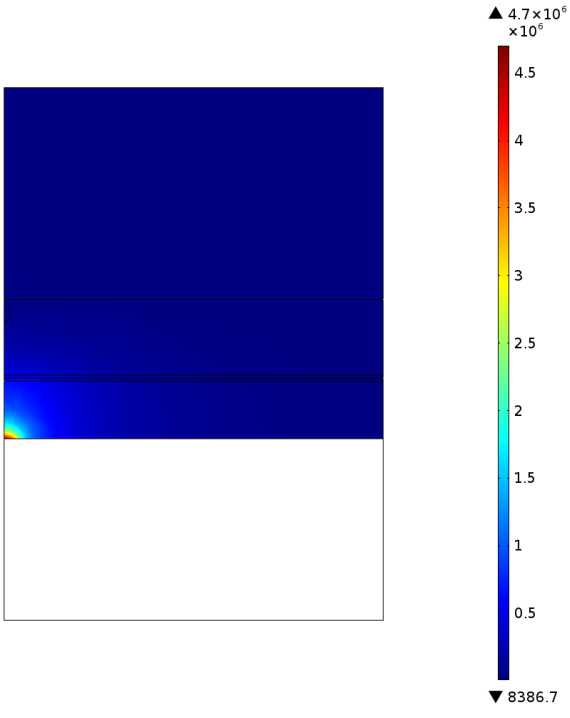

Figure 3: Cut plane through laser path showing a) temperature profile in ^{o}C; b) damaged tissue; c) laser fluence in W/m^2; laser fluence was not modeled in the vitreous section; areas colored red in b) represent damaged tissue after 1 second of heating. A large portion of the retina, CC, RPE, and choroid are damaged after 1 second of laser heating.

The temperature in the center of the feeder vessel is shown in Figure 4 for 1 second of laser heating. Since this point is in the center of the laser path, this should represent the hottest point within the center of the feeder vessel. The temperature increase at the center of the laser application is also shown in Figure 4. Temperatures as high as 70^{o}C were observed within this section and at any time interval, the temperature rise within the retina exceeds the rise in the feeder vessel.

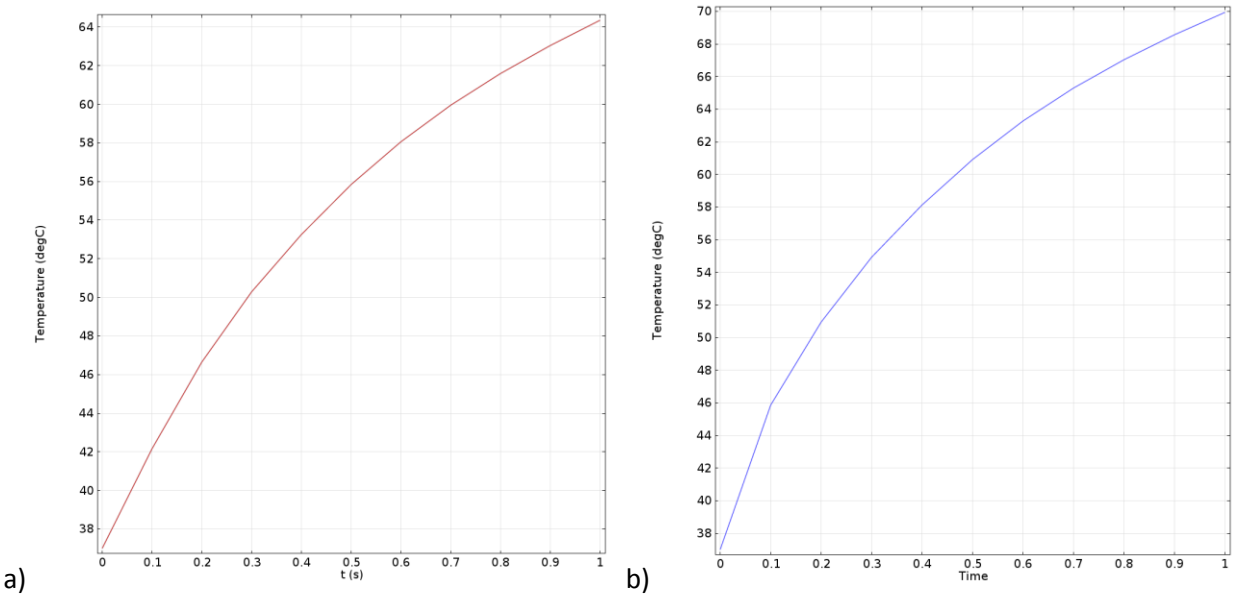

Figure 4: Temperature variation with time after laser application a) in center of feeder vessel: b) in center of laser irradiance surface. The laser spot heats faster than the feeder vessel indicating that damage to other tissue sections will exceed the damage to the feeder vessel.

3.3 Thermal Damage

Thermal damage was assessed in the feeder vessel as well as the RPE section. While thermal damage to the feeder vessel is the goal of the laser photocoagulation treatment, thermal damage should be minimized in other tissue sections. As the RPE section has the highest absorbance of all tissue sections are reaches the highest temperatures, damage in the RPE is taken as a "worst-case" indicator of damage in other tissue sections. A more detailed discussion of how thermal damage was calculated can be found in Appendix A.

The thermal damage within the feeder vessel is maximum within the laser path as this section is directly in contact with the laser energy and hence experiences the most intense temperature rise. Figure 5 shows the variation in thermal damage across the length of the feeder vessel at various times during laser heating. As can be seen, the temperature rise is most dramatic within the RPE and CC sections which reach 86^{o}C after 1 second of heating. Thermal damage begins to occur in the feeder vessel after only 0.4 s of heating.

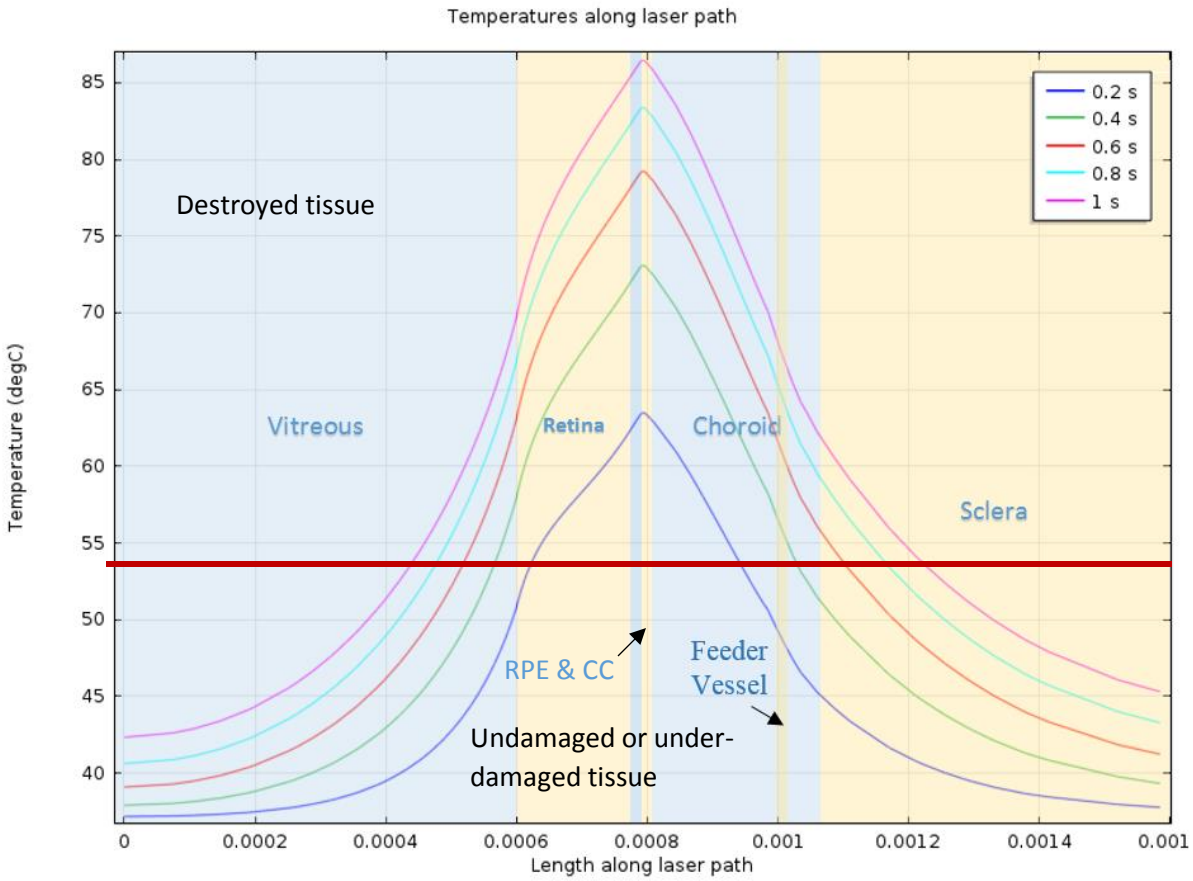

Figure 5: Temperatures along the laser path in different tissue sections. Temperature elevation is quite rapid and occurs primarily in the retina, RPE, CC, and choroid. The feeder vessel begins to be damaged after only 0.4 s of heating.

Temperature elevation in the feeder vessel lags behind other tissue sections as laser energy is absorbed more within the retina, RPE and CC sections, and because heat diffuses through these sections to reach the feeder vessel. Of interest, is the time is takes to completely destroy one cross-section within the feeder vessel. Figure 6 shows the minimum thermal damage within the cross-section of the feeder vessel that was directly in the laser path which represents the cross section of most intense heating. As can be seen in Figure 6, 0.55 seconds is sufficient to inflict the desired damage to the feeder vessel along an entire cross section which should result in successful treatment. Beyond this point, further treatment serves as a margin of safety, ensuring the treatment was successful but also increases the collateral damage to nearby tissue.

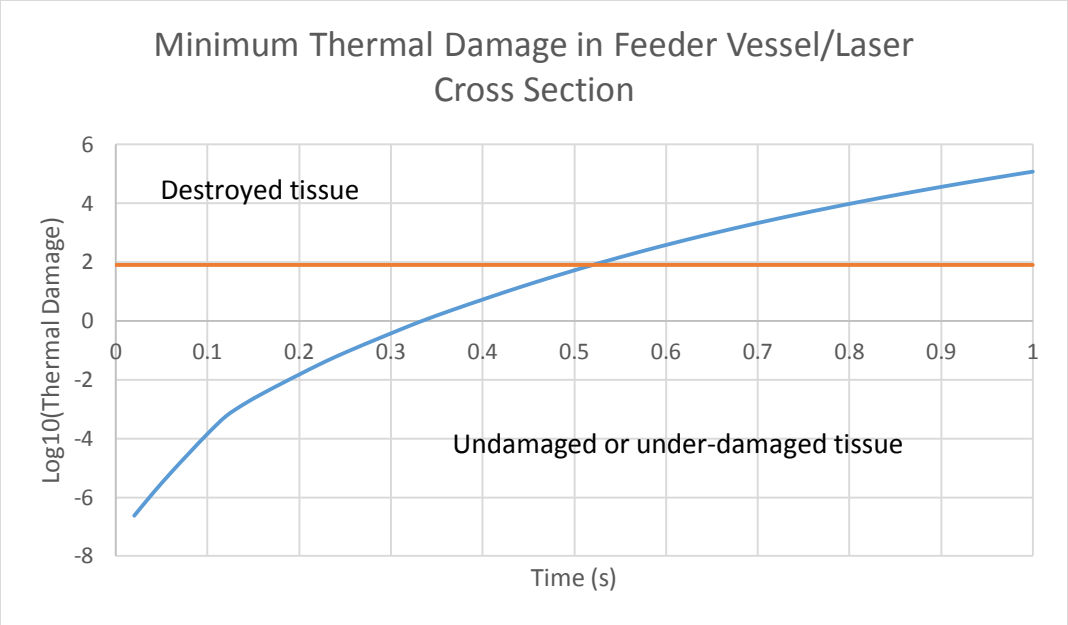

Figure 6: Thermal damage the feeder vessel cross section directly within the laser path. The feeder vessel cross section of interest is destroyed after about 0.55 s of laser heating.

Of interest as well, is the amount of tissue in other sections that are damaged by the laser photocoagulation treatment. Figure 7 shows the percent of tissue within each section that is damaged during treatment (as determined by a CEM43^{o}C > 80). The vitreous and sclera sections incur little damage compared to other tissues. The most severe damage occurs in the RPE and CC sections because of their proximity to the laser application surface, high absorbance values, and thinness relative to other sections. The retina also experiences significant damage of up to 20% of the modeled tissue. Shortening the laser application duration could help reduce damage to other tissue sections.

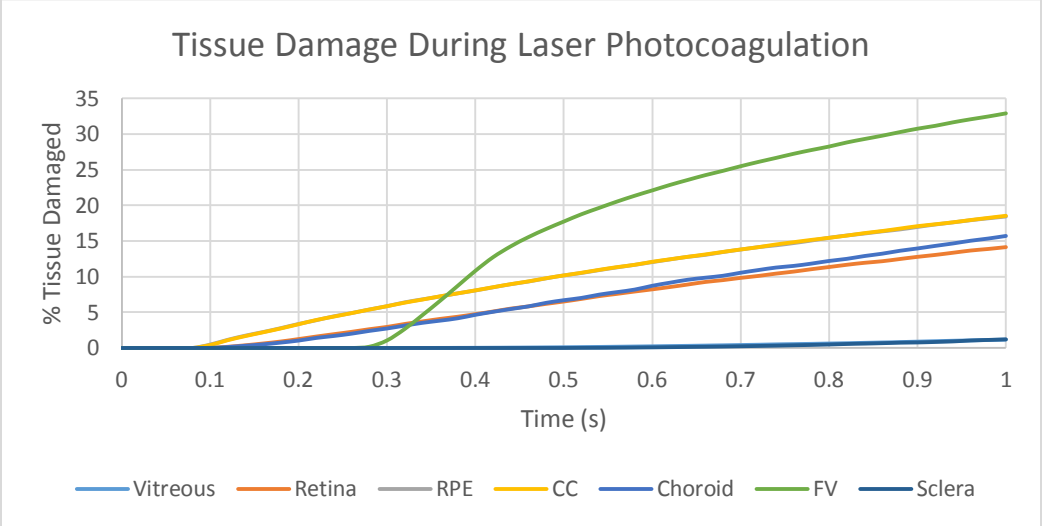

Figure 7: Extent of tissue damage in eye tissue sections. While the feeder vessel has the most damaged tissue after 1 second of heating, other tissue sections are significantly damaged during the treatment. Damage is especially high within the RPE and CC.

4.0 Accuracy Check

Overall, the group's results were comparable with a published model of laser photocoagulation by Zhu et al., (2008). There were, however, significant differences in the implementation and development of the two models. Most notably:

1. Zhu et al. (2008) treated the laser heating as a source term which exponentially decayed through the eye tissue sections. The model presented in this report was developed by solving the laser diffusion equations proposed by Zhang et al. (2005) and using that result to determine the heat source term.
2. The domain presented in this report is much larger than that of Zhu et al. (2008). The domain in the literature consisted of a 1000 µm cylinder which the authors report was sufficient to result in a "less than 0.1% change in the temperature elevation along the central line of the laser beam". Comparatively, the group's model domain was considerably larger, consisting of a width of 2500 µm and height of 3000 µm. Additionally, the vitreous section in the group's model was much shorter as the semi-infinite heat transfer condition was met at a vitreous domain length of 600 µm instead of 2 cm as presented in the report. The temperature elevation on the boundaries far from the laser beam path were maintained at 37^{o}C after 1 second of heating suggesting the semi-infinite condition was met. This was not satisfied for a smaller overall domain as presented in the literature.

Since this model has fundamentally changed the way laser diffusion is modelled, we cannot expect to achieve exact same result as that reported in the literature. Nevertheless, the two models were qualitatively compared as presented below. Figure 8 shows the temperature profile at the same surface from two studies. Our study reaches a slightly lower maximum temperature because of the increased scale of the overall domain which allows more heat to diffuse through the tissue resulting in lower local temperatures. The temperature profile the group obtained is also in line with that reported by Zhu et al. (2008). As with their model, the hottest temperatures are reported in the RPE section where the absorbance is highest. Zhu et al, reported feeder vessel temperatures in the range of 54 to 87^{o}C under various conditions whereas the highest temperature achieved in the feeder vessel was 67^{o}C in the group's model.

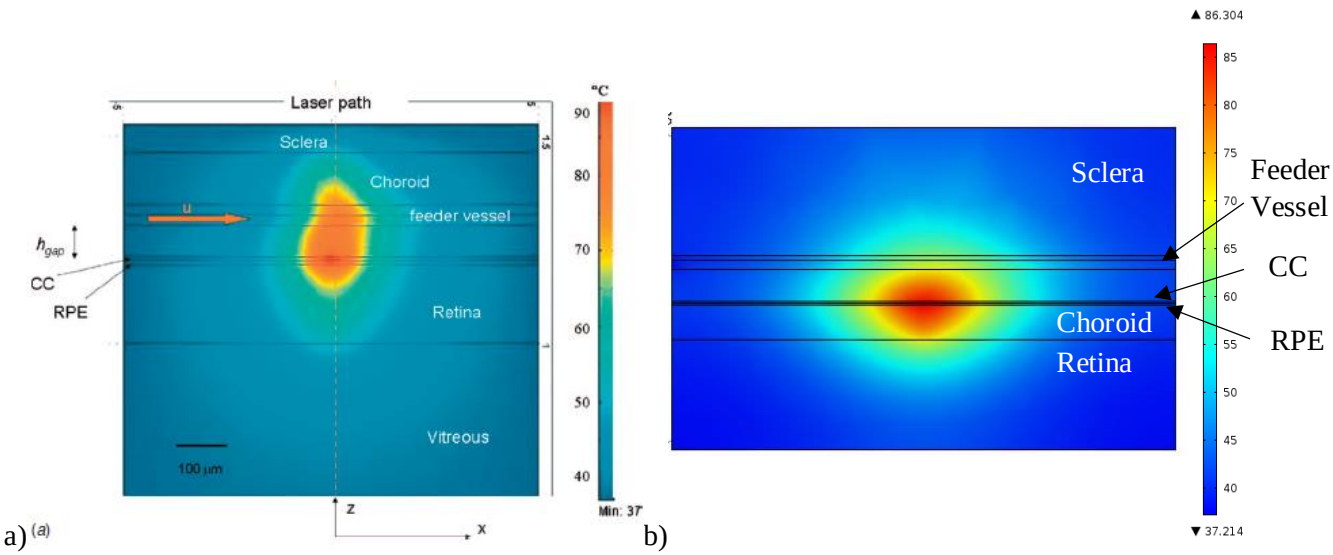

Figure 8: Temperature profile in surface of intense laser heating at t=1s from: a) Zhu et al, 2008 b) the group's model. The temperature profiles a similar but temperatures are lower in the group's model than that reported in the literature. The variation in temperatures is likely due to differences in the model configurations.

The effect of blood velocity on heat transfer was also compared between the two studies. As shown in Figure 9, the difference in maximum temperature can also be explained by the adjusted geometry, but the same trend was observed in both studies, the temperature peak shifts towards the right as blood velocity increases, showing that blood velocity has the same effect on the two models. The magnitude of this effect is comparable in the two studies.

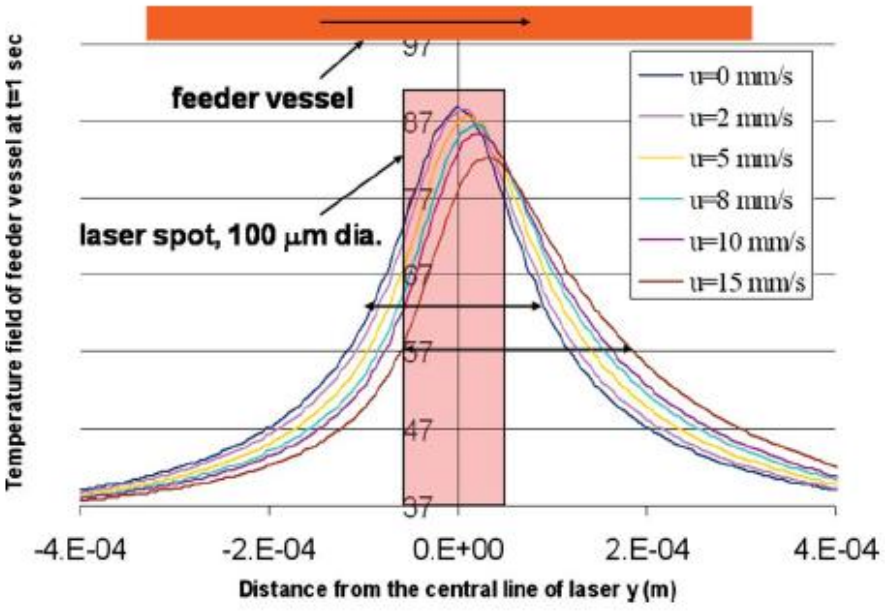

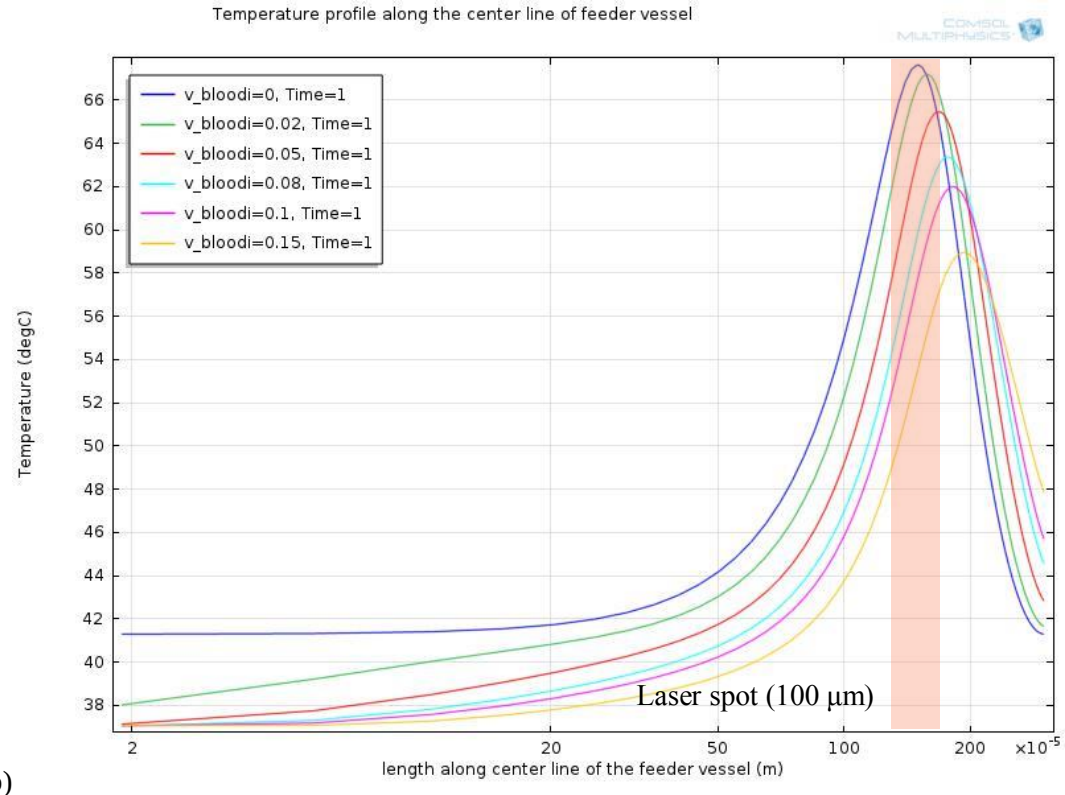

b)

Figure 9 a) Lateral temperature distributions in the axial direction of the feeder vessel for different blood velocity; b) temperature distributions along the length of feeder vessel for different blood velocity. Increasing blood velocity shows the same trend in both models. Increasing blood velocity reduces the maximum temperature in the feeder vessel and shifts this maximum upstream.

5.0 Sensitivity Analysis

Sensitivity analysis was conducted for thermal properties (k, ρ, c_p) in different tissue layers. Different values of k, ρ, and c_p were reviewed for each layer of tissue from 5 independent sources (White et al, 1970; Amara, 1995; Ng&Ooi, 2006; Narasimhan et al, 2010; Buccella et al, 2007). Mean, μ, and standard deviation, σ, were then calculated based on those findings. The range of sensitivity analysis for each parameter input is (μ - 2σ, μ + 2σ). The determined range is summarized in the table below:

Table 1: Property ranges for thermal property sensitivity analysis

	k (W/mK)		**ρ (kg/m^3)**		**c_p (J/kgK)**	
	lower bound	upper bound	lower bound	upper bound	lower bound	upper bound
Vitreous	0.570593	0.611807	995	1011	4047	4256.6
Retina	0.414114	0.686506	976.9478	1068.052	3439.519	4472.681
RPE	0.495154	0.689146	916.0756	1193.924	2950.177	4731.903
Choriocapillaris	0.402103	0.830377	916.0756	1193.924	3540.259	4317.281
Choroid	0.402103	0.830377	916.0756	1193.924	3540.259	4317.281

Feeder vessel	0.474843	0.598491	984.1733	1089.16	3440.273	4356.394
Sclera	0.385867	1.207733	971.3596	1213.64	2675.26	4693.66

Sensitivity analysis results were assessed for the temperature at the center of the feeder vessel at t = 1 s by varying parameters such as thermal conductivity (k), specific heat capacity (c_p), and density (ρ). The baseline temperature of center of the feeder vessel, which is the temperature computed with no variations in any parameters, was 64.3537°C.

Table 2: Sensitivity analysis results for different physical parameters in the RPE and feeder vessel

	k_RPE (W/mK)	**k_FV (W/mK)**	**ρ _RPE (kg/m^3)**	**ρ _FV (kg/m^3)**	**c_p_RPE (J/kgK)**	**c_p_FV (J/kgK)**
Low value	0.495154	0.47484	916.076	984.173	2950.177	3440.273
Model value	0.6276	0.52	1170	1060	3096.16	3617
High value	0.689146	0.59849	1193.92	1089.16	4731.903	4356.394
Result (low parameter value, °C)	64.3925	64.2612	64.3863	64.4444	64.3608	64.4161
Result (high parameter value, °C)	64.3363	64.4992	64.3506	64.3177	64.2749	64.0713
Percent difference, low (%)	0.0603	-0.144	0.0507	0.141	0.011	0.097
Percent difference, high (%)	-0.0271	0.226	-0.005	-0.056	-0.122	-0.439

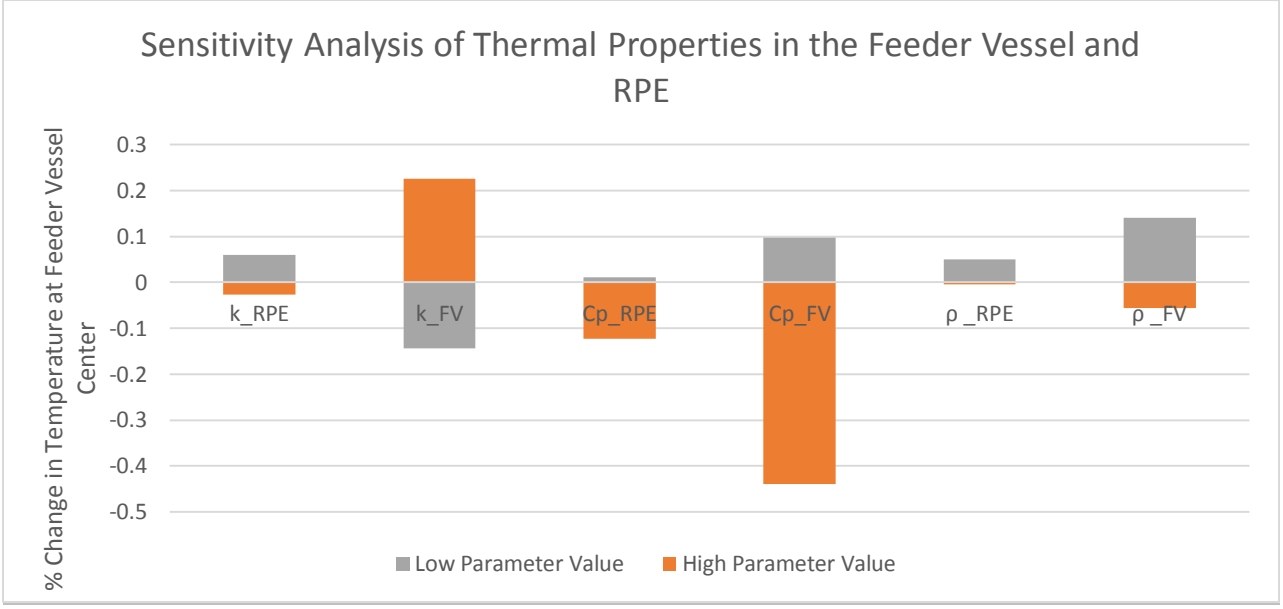

Figure 10: Sensitivity Analysis of low and high physical parameters in RPE and Feeder Vessel. Results were found to have little sensitivity to thermal parameters, suggesting good applicability in different patients.

Data for optical property (μ_a, absorption coefficient) of human tissue is scarce, but it is noted that variability in optical parameters can be as high as 20% (Hammer, 1994). Therefore, the

sensitivity analysis of the attenuation factor, will be varied by +/-20%. Figure 11 summarizes the results of sensitivity analysis with respect to optical parameters in RPE and feeder vessel sections.

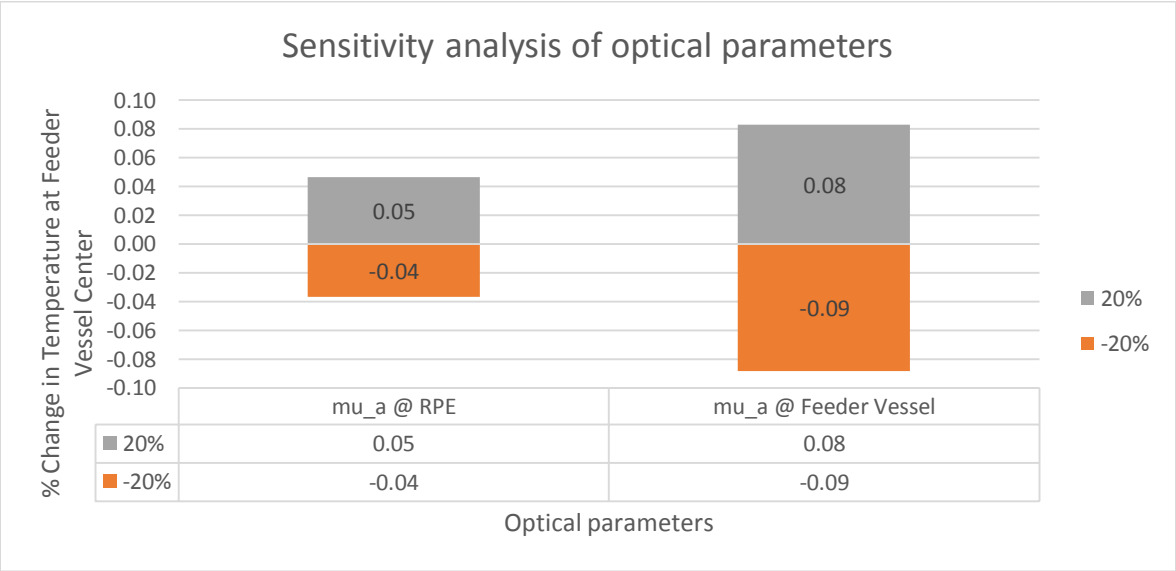

Figure 11: Sensitivity analysis results for optical parameters in RPE and feeder vessel sections. Results were found to have little sensitivity to laser absorbance, suggesting good applicability in different patients.

Despite of the relatively large variation of absorption coefficient, the percentage change in temperature at the center of feeder vessel at t = 1 s is very small. Variation in μ_a was expected to greatly change the distribution of laser fluence among sections and consequently change the pattern of initial heat absorption but this was not significantly observed. The results suggest that this model is more responsive to the change of absorption coefficient in the feeder vessel. In general, this model is quite robust to the variation in optical parameters among individuals, which is quite common according to clinical study.

6.0 Optimization

Several variables were considered to optimize the laser photocoagulation process including the effect of blood flow velocity within the feeder vessel, injection of high-absorbance dye into the feeder vessel for improved heat transfer, and varying the laser heating duration. The model was assessed under each condition with results presented in sections 5.1, 5.2, and 5.3 below.

6.1 Effect of Blood Flow Velocity

To assess the effect of blood flow velocity in the feeder vessel on the temperature profile in the eye, the temperature profile was recalculated under various blood flow velocities. This is presented below in Figure 12.

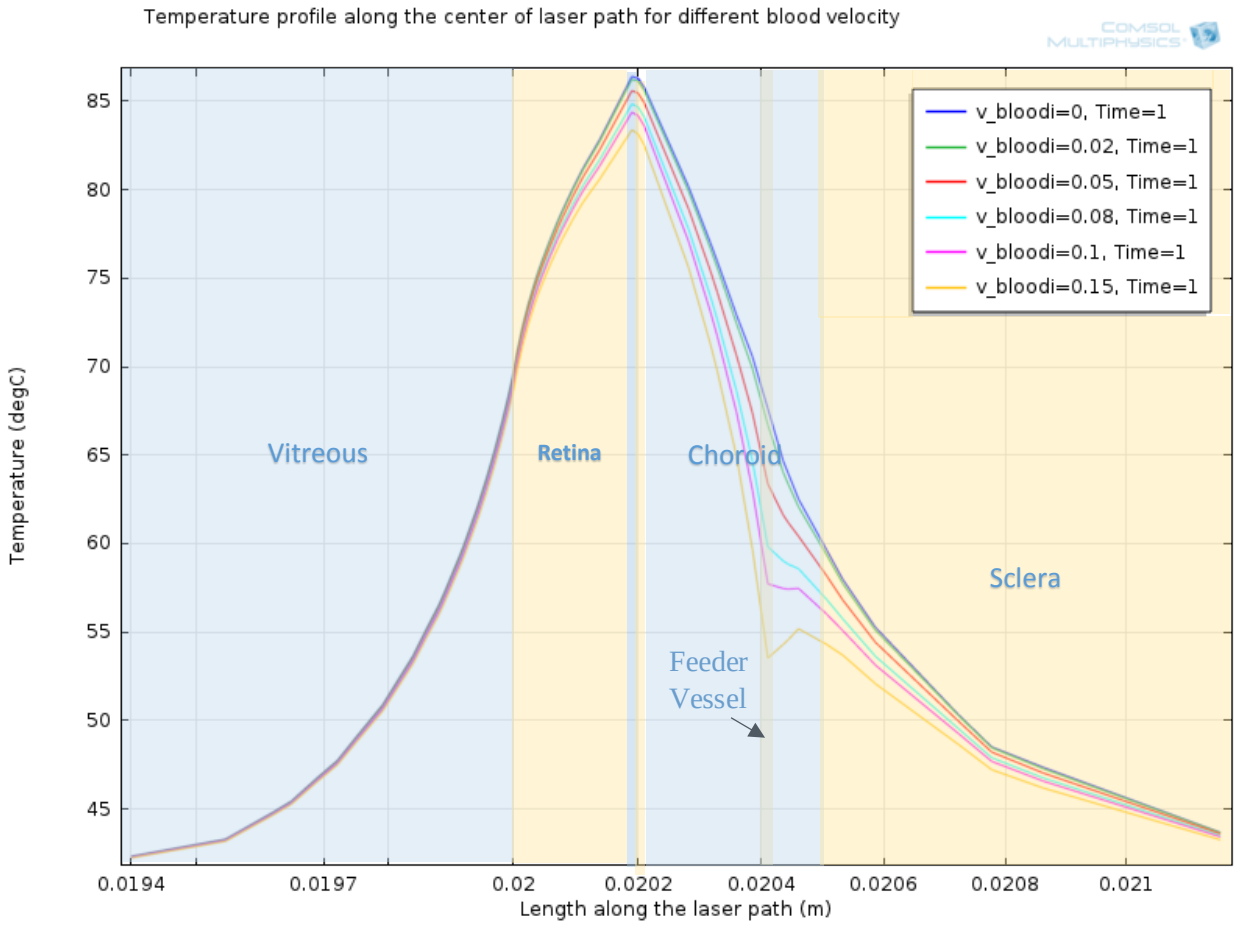

Figure 12: Various Temperature Profile along the center of the laser path for different blood velocity. Increasing blood velocity reduces the temperature in the feeder vessel.

Increased blood flow velocity tended to reduce the temperature within the feeder vessel as relatively cooler blood convected away incident laser heat. This effect is most pronounced at a velocity of 0.15 m/s where the temperature in the feeder vessel actually falls below that of the adjacent tissue sections. As would be expected, low blood flow velocity increases the efficacy of the laser photocoagulation treatment by allowing for increased local temperatures within the feeder vessel by reduced convection.

6.2 Dye Assisted Photocoagulation

Dye assisted photocoagulation was modeled as a shift in the absorbance, μ_a, of the feeder vessel from a value of 4610 m^{-1} to 9000 m^{-1} as reported by Zhu et al (2008). The increased absorbance affects the laser absorbance within the feeder vessel, tending to greater absorbance of laser energy and reduced diffusion of laser energy within the feeder vessel. Additionally, since the heat source term is linearly proportional to the absorbance, the near doubling of the feeder vessel absorbance should substantially increase the heat generation within the feeder vessel. Surprisingly, the dye assisted photocoagulation model was very close to original results with a maximum increase in temperature of only 0.5% within the feeder vessel as illustrated in Figure

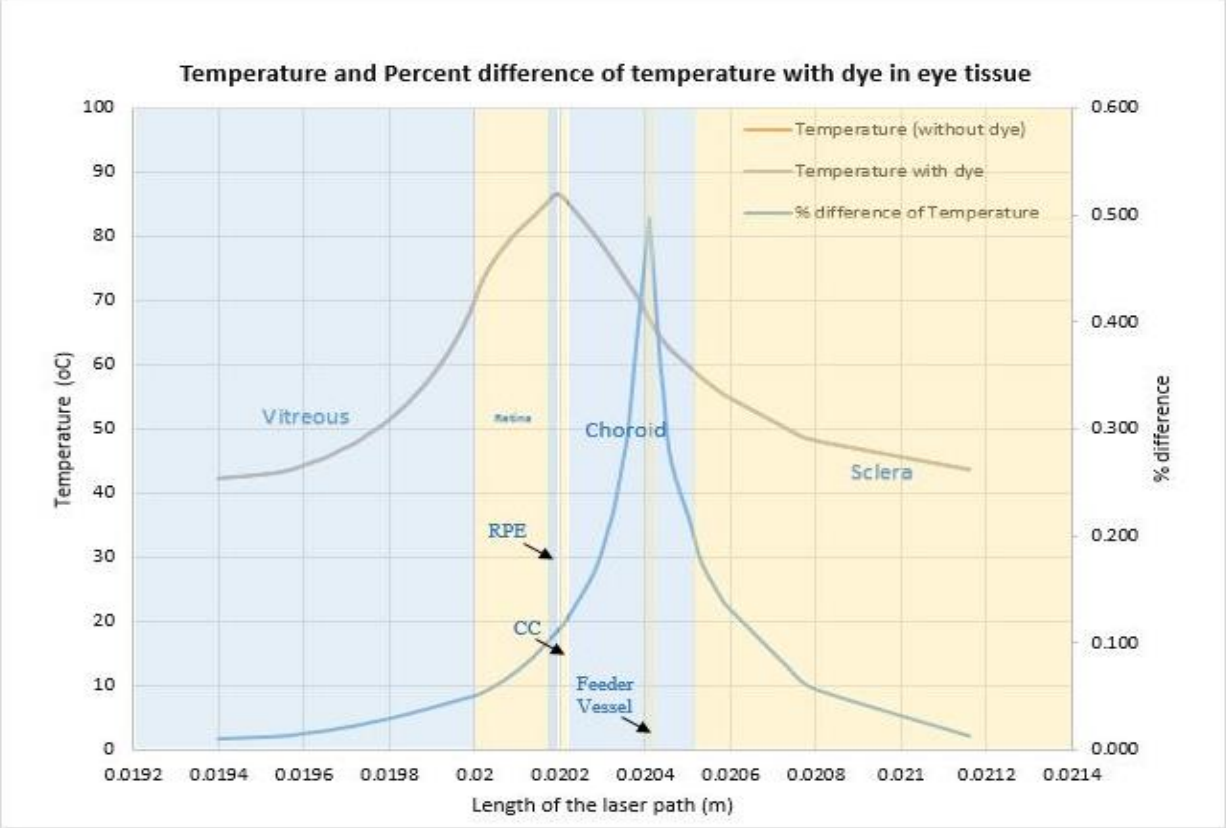

13.

Figure 13: Temperature and percent difference of temperature with dye in each section of the eye tissue. Dye assisted photocoagulation was found to have little effect on temperature elevation within the feeder vessel.

These results suggest that dye assisted photocoagulation, while useful, does not make a large difference in the thermal profile obtained from laser heating. However, these results do suggest that any mechanism to increase absorbance within the feeder vessel will have an effect on the efficacy of treatment by increasing heating within the feeder vessel.

6.3 Effect of Laser Heating Duration

The results from this study illustrate the intense and rapid heating that occurs within the eye during laser photocoagulation. The photocoagulation process may be considered successful when a single cross-section within the feeder vessel is completely destroyed, and, as was seen from

Figure 6, this occurred after 0.55 s of laser application. After this point, additional laser heating acts as a margin of safety, ensuring adequate destruction of the feeder vessel but also incurs the negative side effect of additional collateral tissue damage. As was seen from the sensitivity analysis, variation in thermal and dielectric properties cause very little variation in the temperatures in the feeder vessel. What has not been studied however, is the effect of varying tissue geometry on the thermal profile which may have a large impact on the efficacy of shorter treatments. It is difficult to judge the optimized treatment time for a varied population from this study alone however this model suggests that 0.55 seconds is the minimum time to destroy the feeder vessel. An application of 1 second may therefore be reasonable to account for variations in individual eye geometries and properties.

7.0 Conclusions

This study provided insight into the heat transfer that occurs during laser photocoagulation for treatment of AMD related CNV. From the results it is evident that damage to the RPE is great concern during treatment as this section experiences the most rapid rise in temperature due to its high absorbance of laser energy. So long as the absorbance of the feeder vessel is less than the RPE section, the RPE section will experience greater thermal damage for a given treatment. A possible solution to this problem would be the use of dye injection which increases the absorbance within the feeder vessel. However, as shown in the Optimization section of this report, nearly doubling the absorbance of the feeder vessel does not change the temperature within the feeder vessel by much, only 0.5%. The use of more highly absorbent dyes may improve the overall therapy.

From the thermal damage results, it is clear that a temperature of $43^{o}C$ is reached within the hottest section of the feeder vessel extremely rapidly. The desired thermal damage within the feeder vessel is also reached within 0.55 s, suggesting that treatment may stop after this time. However, to ensure that photocoagulation is successful, laser application should still exceed 0.55 seconds and this result may inform future laser treatments. This study did not explore the effect of variation in eye tissue geometry which would likely have a large effect on the temperature rise in the feeder vessel. Considering the wealth of factors that could undermine the efficacy of treatment, a laser duration of 1 second is reasonable to ensure complete destruction of the target tissue. In practice, treatment times vary considerably, from 0.1 to 60 seconds, depending on the laser type, patient, and particular treatment. Further studies are needed to extend these results to other treatments and lasers. As well, studies will need to explore the variability in eye tissue and how this may affect different treatment options. Later studies could also investigate the application of even more absorbent dyes to improve targeting heating within the feeder vessel as well as the application of more powerful lasers and different laser application methods like pulsing.

8.0 Acknowledgements

The group would like to thank Prof. Ashim Datta, Alex Warning, Dr. Traci Nathans-Kelly, and Dr. Rick Evans for their time, advice, and feedback. This project would not have been possible without their guidance and continued support.

Appendix A: Mathematical Formulation

Geometry

The model was created in 3D Cartesian geometry with domains represented as concatenated slabs. The height and width of the model were selected to simulate semi-infinite conditions which were validated as no heat transfer is observed on the far ends of the model domain.

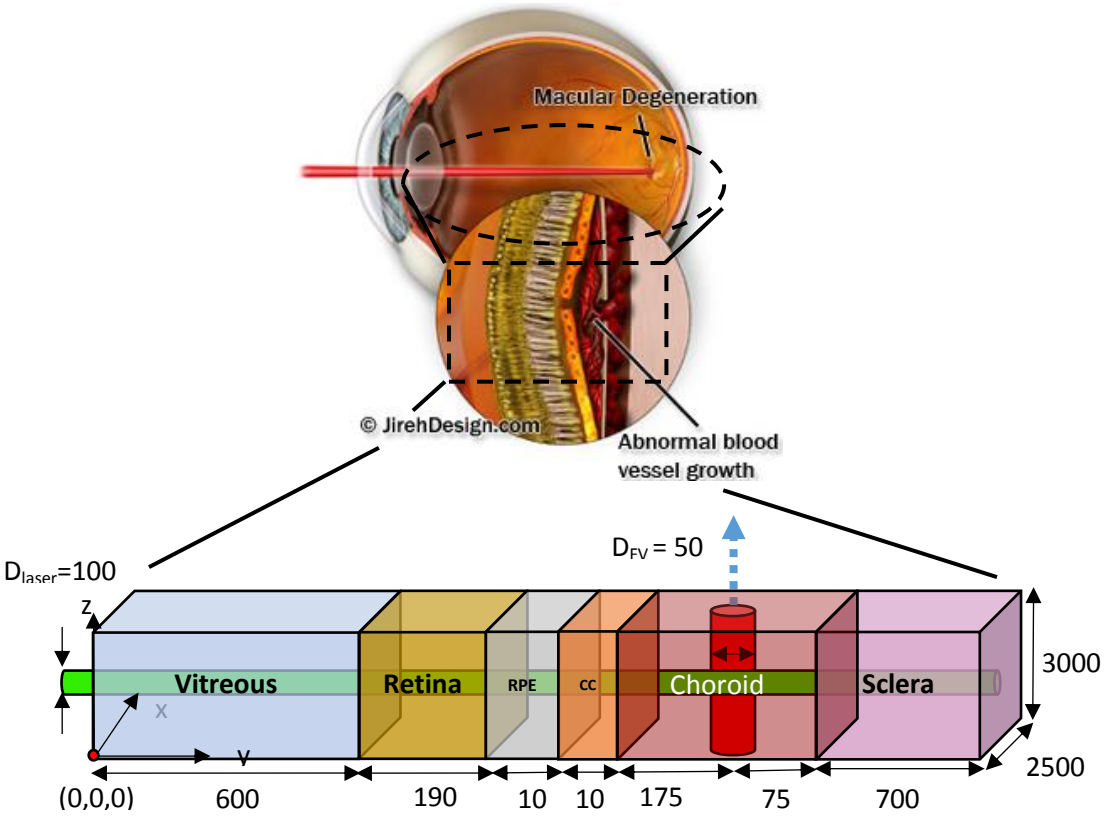

Figure 15: Schematic of CNV in eyeball (source: http://maculacenter.com/macular-degeneration/cnvm/) and a geometry of 3D heat transfer in Cartesian coordinates is set up for the region of our interest. All dimensions in µm.

Laser and feeder vessels are centered at (500, 500, z) and (500, y, 2410), respectively. Blood flow through the feeder vessel occurs in the positive z direction as indicated by the blue arrow. The problem is assumed to be symmetric about the y-z plane that cuts through the center of the feeder vessel. The diagram is displayed with both sides of symmetry for clarity but the COMSOL model geometry represents only half the geometry displayed above, to a width of 1275 µm.

To better simulate the laser heating, the laser is assumed to be applied directly at the retina as a 5% loss in laser power was assumed for laser heat which is dissipated through the vitreous section. The 5% loss corresponds to energy lost in the form of heat within the vitreous section and was determined by applying an exponential decay function as a heat source term within the vitreous section as done by Zhu et al. (2008).

Governing Equations

The model was solved for laser diffusion, heat transfer, and laminar flow in the feeder vessel.

Heat transfer:

In different tissue layers:

$$\rho c_p \frac{\partial T_t}{\partial t} = k_t \frac{\partial^2 T_t}{\partial x^2} + k_t \frac{\partial^2 T_t}{\partial y^2} + k_t \frac{\partial^2 T_t}{\partial z^2} + q_{laser} \ (A.1)$$

where ρ is the density, c_p is the specific heat, T_t is the temperature of each layer temperature, q_{laser} is the laser heat generation in volumetric term in [W/m^3].

In the feeder vessel:

$$\rho c_p \frac{\partial T_f}{\partial t} + u\rho c_p \frac{\partial T_f}{\partial z} = k_t \frac{\partial^2 T_f}{\partial x^2} + k_t \frac{\partial^2 T_f}{\partial y^2} + k_t \frac{\partial^2 T_t}{\partial z^2} + q_{laser} \ (A.2)$$

where u is the average blood flow velocity in the feeder vessel

The flow field was initially solved using equation 3.6 below, however due to the thinness of the feeder vessel and subsequently small velocity gradient within, the model was later simplified by assuming plug flow within the feeder vessel, at a constant velocity.

Laser diffusion:

The heat source term used in equation 3.1 and 3.2 was computed from the light diffusion model proposed by Zhang et al. (2005), where:

$$q_{laser} = \mu_a \phi \ (A.3)$$

Laser fluence, ϕ[W/m^2], which is the rate of the incident laser light, is given by the diffusion equation also proposed by Zhang et al. (2005) but under steady state conditions:

$$-D\nabla^2\phi + c_*\mu_a\phi = 0 \ (A.4)$$

$$\mathrm{D} = \mathrm{c}_*[3(\mu_a + (1-g)\mu_s)]^{-1} \ (A.5)$$

D [m^2/s]: Optical diffusion coefficient of skin

c_* [m/s]: Speed of light in the particular tissue component

g: Optical anisotropy factor

For laser heating, g is assumed to be very close to 1 (Zhu et al., 2008). This reduces the diffusivity to:

$$\mathrm{D} = \mathrm{c}_*/3\mu_a \ (A.6)$$

To validate the steady state assumption for the laser fluence, the diffusion through the tissue sections was estimated and compared with the length of each section. Table 3 shows the results

of these calculations. A value much less than one for the ratio, $\boldsymbol{L^2/\frac{c^*}{3\mu_a c_0^*}}$, indicates that diffusion happens extremely quickly through the tissue and validates a steady state assumption. This assumption was also validated by comparing transient and steady state solutions which found results to be within 1% of each other.

Table 3: Comparison of diffusion areas in tissue sections to validate the steady state approach to modeling laser fluence. A ratio less than 0.1 suggests that diffusion distance is much larger than the tissue length, validating a steady state approach

Tissue Section	Length (μm)	μ_a (m^{-1})	c* (m/s x 10^7)	$L^2/\frac{c^*}{3\mu_a c_0^*}$ (m)
Vitreous	2000	2.56	2.94	0.000313253
Retina	190	725	3	0.000784632
RPE	10	14000	3	4.19709E-05
CC	10	2040	3	6.11577E-06
Choroid 1	125	3500	3	0.00163949
Feeder Vessel	50	4610	3.08	0.000336537
Choroid 2	50	3500	3	0.000262318
Sclera	700	506	3.82	0.005837477

Laminar flow:

Blood flow in the feeder vessel is modeled as incompressible, Newtonian, flow satisfying the Navier-Stokes equation in the z-direction:

$$\rho\frac{\partial u_z}{\partial t} = \mu\left[\frac{\partial^2 u_z}{\partial x^2} + \frac{\partial^2 u_z}{\partial y^2}\right] - \frac{\partial P}{\partial z} \quad (A.7)$$

u_z [m/s]: blood velocity in feeder vessel (in z direction only)

Boundary Conditions

Since the scale of our model is much bigger than the diffusion of laser energy, we assume zero flux at all system boundaries since they are far enough away from the heat source to not be affected by heat diffusion.

Heat Transfer

No flux boundary condition on all external domain boundaries:

$$\vec{n}\cdot(-k\nabla T) = 0 \text{ (A.8)}$$

Blood inflow in the feeder vessel was assumed to be at body temperature, 37°C. The feeder vessel inlet boundary was subject to the condition:

$$\vec{n}\cdot(-k\nabla T) = q''_{blood} \text{ (A.9)}$$

Laser Fluence

No flux boundary condition on all external domain boundaries:

$$-D\frac{\partial \phi}{\partial n} = 0 \text{ (A.10)}$$

The incident laser light was modeled as a constant flux boundary condition given below:

$$I_{\lambda_0}(x,z)\mathrm{c}_0 = -D\frac{\partial \phi}{\partial n} \text{ (A.11)}$$

Where: I_{λ_0}(x,z) [W/m^2] is the laser irradiance, n: normal direction

c_0 [m/s] = the speed of light in vacuum

To better simulate the laser heating, the laser was assumed to pass directly through the vitreous section and thus was modeled as being applied directly at the retina. Zhu et al. (2008), modeled laser heating as a volumetric source term which decayed exponentially through each tissue section. As per their work, the laser application at the retina was assumed to be attenuated by a factor of about 5% which was determined by calculating the heat generated from laser heating within the vitreous section and subtracting this from the incident energy.

$$Q_{vitreous,loss} = I_{\lambda_0}(1 - e^{-\mu_{vitreous}t_{vitreous}}) = I_{\lambda_0}(1 - e^{-2.56\ m^{-1}*0.02\ m}) = 0.05I_{\lambda_0} \text{ (A.12)}$$

As most lasers do not generate constant flux across the entire beam radius, the laser was modeled as a Gaussian beam which exponentially decays in intensity with distance from the beam center. Thus the laser irradiance was given as:

$$I_{\lambda_0} = e^{-\mu_{vitreous}t_{vitreous}} I_0 e^{-r^2/W_l^2} \text{ (A.13)}$$

Where W_l [m], is the e^2 laser diameter, and $t_{vitreous}$ is the thickness of the vitreous section, 2 cm.

Laminar Flow

For the laminar flow equation within the feeder vessel, a no-slip boundary condition applied on the boundary, meaning that fluid at the surface of vessel wall has zero velocity. This is given by:

$$u_z = 0 \text{ (A.14)}$$

Inflow was modeled as a constant inlet velocity, given by:

$$u_z = v_{in} \text{ (A.15)}$$

Outflow was given by assuming zero pressure at the outlet, thus:

$$P_{out} = 0 \text{ (A.16)}$$

Initial Conditions

The initial temperature of all computation domains is 37^{o}C
Initial laser fluence is zero in all computational domains.
The initial blood velocity varies between 0 and 0.15 m/s, unless otherwise specified, computations were performed for a blood flow velocity of 0.02 m/s.

Initial blood pressure is 2304.5 Pa

Thermal Damage

Determining the extent of thermal damage to tissue can be difficult as several models exist. For this study, thermal damage of tissue was assessing by determining the isoeffect of short duration heating compared to long term heating at a temperature of 43^{o}C. The cumulative equivalent number of minutes at 43^{o}C (CEM43^{o}C) was determined using an equation proposed by Dewhirst et al. (2003):

$$CEM43^{o}C = tR^{43-T} \quad \text{(A.17)}$$

Where t is the time tissue has been subjected to a particular temperature, T, and R the number of minutes needed to compensate for a 1^{o}C temperature change. For successful removal of the feed vessel, CEM43^{o}C should be at least 80 minutes, based on data for retinal tissue necrosis (Dewirst et al., 2003). R is dependent on whether or not the tissue is above the damage "breakpoint". For *in vitro* human tissue the R value suggested by Dewhirst et al. is 0.233 (T < 43.5^{o}C) and 0.428 (T > 43.5^{o}C).

As temperatures are increasing very rapidly in the modeled tissue, the extent of thermal damage was estimated by assessing which volumes of tissue were at a temperature greater than 53.8^{o}C. This temperature was chosen because it corresponds to a duration of 0.5 s to achieve the CEM43^{o}C isoeffect of 80 minutes. It was assumed that if tissues reached this temperature at any instant, even at the end of laser application when temperatures begin to fall, that it would be reasonably maintained for 0.5 s within that tissue section to induce necrosis.

Input Parameters

Thermal and dielectric properties of eye tissue and blood are included in Table 4 and other parameters included in the model in Table 5. Thermal properties were taking from various sources within the scientific literature. The speed of light in various tissue sections has been calculated from permittivity and permeability values found in literature and used at a frequency of 100 MHz, this will need to be corrected to account for the laser frequency. Where unavailable, the speed of light was estimated to be 3*10^{7} m/s to closely match the speed of light in other tissue sections. These properties are marked with an asterisk.

Table 4: Thermal and dielectric properties of eye tissue used in the model

	Density (kg/m^{3})	**Thermal Conductivity (W/mK)**	**Specific Heat Capacity (J/kgK)**	**Absorbance (m^{-1})**	**Speed of Light (x 10^{-7} m/s)**	**Viscosity (x 10^{-3} Pa-s)**
Vitreous	1005[a]	0.59[a]	4047[a]	2.56[b]	2.94[c]	
Retina	1040[a]	0.46024[a]	3556.4[a]	725[b]	3.00*	
RPE	1170[a]	0.6276[a]	3096.16[a]	14000[b]	3.00*	
Choriocapillaris	1170[a]	0.79496[a]	3640.08[a]	2040[b]	3.00*	
Choroid	1170[a]	0.79496[a]	3640.08[a]	3500[b]	3.00*	
Feeder Vessel	1060[a]	0.52[a]	3617[a]	4610[b]	3.08[c]	3[d]

Feeder Vessel w/dye	1060[a]	0.52[a]	3617[a]	9000[b]	3.08[c]	3[d]
Sclera	1100[a]	1.00416[a]	3179.84[a]	506[b]	3.82[c]	

[a] White et al., 1970; [b] Zhu et al., 2009; [c] IT'IS foundation, 2013; [d] Merril et al., 1963; (* estimated values)

(*estimated values)

Table 5: Model properties

Property	Description	Value	Unit
W_l	Laser e^2 diameter	50	μm
I_0	Laser fluence rate	637	W/cm^2
c_{light0}	Speed of light in vacuum	3.00E+08	m/s
v_{bloodi}	Blood velocity in feeder vessel	0.02	m/s

Appendix B: Solver Configurations and Meshing

Solver Configurations

To simplify calculations and reduce the calculation time, each physics (laminar flow, heat transfer, and laser fluence) were solved individually in separate studies with solutions passed to the next study as needed using COMSOL's default feature. Temperature studies were solved using COMSOL's direct, PARDISO solver. Laser fluence calculations were attempted to be solved using the iterative solver but it was unable to converge. This was switched to the direct solver which gave satisfactory solutions using the MUMPS solver.

The time step used for all studies was 0.1 s. To study the effect of laser heating duration on thermal damage in the feeder vessel, the time step was reduced to 0.01 seconds to give better resolution of the transient solution. The relative tolerance for the heat transfer study was 0.01 and 0.001 for the absolute tolerance, as per COMSOL's default setting. For laser fluence the relative tolerance was 0.001. None of these values were changed from their defaults by the group.

Mesh Selection and Mesh Convergence

The mesh was developed as free tetrahedral over all domains and refined in the feeder vessel domain and the surface of the laser application. Each region within the eye is modeled as a separate domain with the laser application taking place along the hemispherical surface shown in Figure 16b and d. The problem is considered to have reflective symmetry about the yz-plane and so only one half of eye was modeled. Meshing is coarse in the vitreous section and increasingly fine in the smaller domains, feeder vessel, and on the laser application surface. The total height and width of the computational domain is 1.5 mm which is much larger than the feeder vessel and thicknesses of RPE, CC, choroid, and sclera sections. This was deemed sufficiently large to be considered semi-infinite for the computation carried out in COMSOL. The complete mesh used to obtain the solution consisted of 23594 domain elements, 8578 boundary elements, and 944 edge elements.

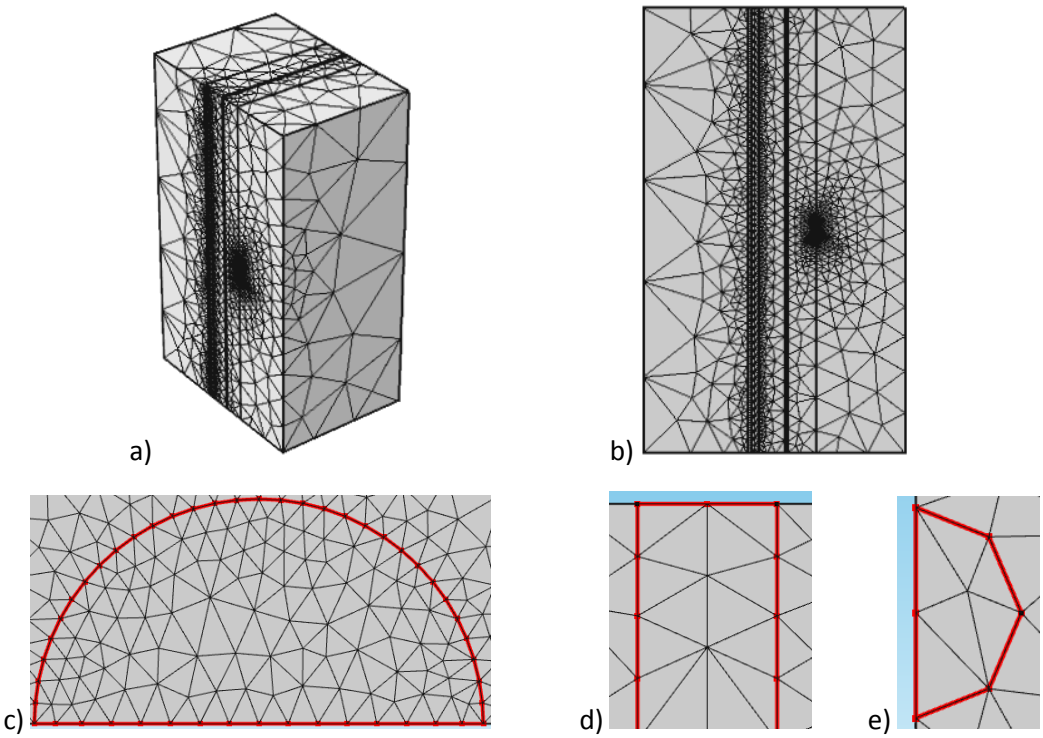

Figure 16: COMSOL model of computational domain showing a) full domain; b) Longitudinal surface, yz-plane; c) close up of laser application surface on xz-plane; d) close up of feeder vessel in yz-plane; e) close up of feeder vessel in xy-plane. The complete mesh consists of 23594 elements. Mesh is finest near the laser spot as temperatures are changing rapidly within this region.

Mesh convergence was established by varying the mesh at the laser application surface and assessing the effect of more refined mesh on the laser fluence within the feeder vessel. This surface was chosen because the laser fluence gradient is greatest in the region of laser application and hence requires the high resolution to be accurately modeled. While temperatures in the feeder vessel are the main interested for this study, laser fluence was used to establish mesh convergence since it determines the heat generation within the tissue and so if the laser fluence was converged within the feeder vessel it is reasonable to assume the temperature will also converge.

A plot of the laser fluence in the feeder vessel center for different mesh sizes is shown in Figure 17. There is very little difference between Solution 5 and 6 and so no further mesh refinement was assessed after Solution 6. Further studies were performed using the mesh size established in Solution 6.

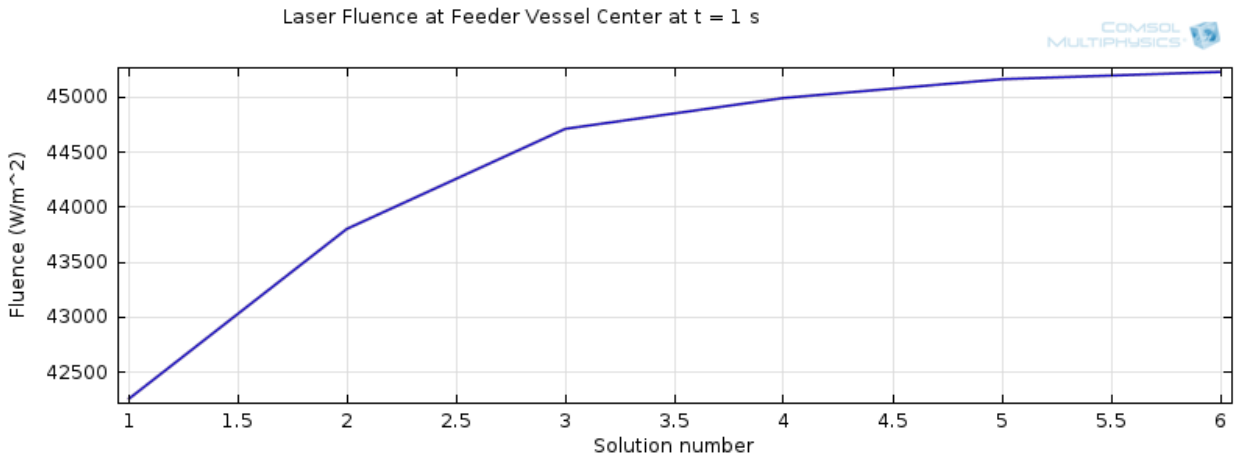

Figure 17: Laser fluence in center of feeder vessel with various mesh sizes. Explanation of mesh sizes is available in Table 6. Mesh size 6 was used for the model as results were found to not change with increasing mesh after this point.

Table 6: Mesh parameters for mesh convergence

Solution Number	Domain elements	Boundary elements	Edge elements
1	17575	6919	862
2	17723	6918	867
3	17983	7053	875
4	18316	7167	886
5	19147	7412	897
6	23594	8578	944

References

Al-Shemmeri, Tarik (2012). Engineering Fluid Mechanics. Ventus Publishing ApS. pp. 17–18.

Amara, E. H. (1995). Numerical investigations on thermal effects of laser-ocular media interaction. International Journal of Heat and Mass Transfer, 38(13), 2479-2488.

Buccella, C., De Santis, V., & Feliziani, M. (2007). Prediction of temperature increase in human eyes due to RF sources. Electromagnetic Compatibility, IEEE Transactions on, 49(4), 825-833.

Complications of Age-Related Macular Degeneration Prevention Trial Research Group. (2006). Laser Treatment in Patients with Bilateral Large Drusen. *American Academy of Ophthalmology*, 113:1974-1986.

Dewhirst, M. W., Viglianti, B. L., Lora-Michiels, M., Hanson, M., Hoopes, P. J. (2003). Basic principles of thermal dosimetry and thermal thresholds for tissue damage from hyperthermia. Int J Hyperthermia. 19(3):267-94.

Gass J. D. (1994). Biomicroscopic and histopathologic considerations regarding the feasibility of surgical excision of subfoveal neovascular membranes. Am J Ophthalmol. 118:285–98.

Hammer, M., Roggan, A., Schweitzer, D., & Muller, G. (1995). Optical properties of ocular fundus tissues-an in vitro study using the double-integrating-sphere technique and inverse Monte Carlo simulation. *Physics in medicine and biology*, *40*(6), 963.

IT'IS Foundation. (2013). *Thermal and dielectric properties.* Retrieved from http://www.itis.ethz.ch/itis-for-health/tissue-properties/downloads/

Lewis, H. (1998). Subfoveal choroidal neovascularization: is there a role for submacular surgery?. American journal of ophthalmology, 126(1), 127.

Merrill, E. W., Gilliland, E. R., Cokelet, G., Shin, H., Britten, A., & Wells Jr, R. E. (1963). Rheology of human blood, near and at zero flow: effects of temperature and hematocrit level. Biophysical Journal, 3(3), 199-213.

Moritz, A. R., & Henriques Jr, F. C. (1947). Studies of Thermal Injury: II. The Relative Importance of Time and Surface Temperature in the Causation of Cutaneous Burns. The American Journal of Pathology, 23(5), 695.

Ng, E. Y. K., & Ooi, E. H. (2006). FEM simulation of the eye structure with bioheat analysis. Computer methods and programs in biomedicine, 82(3), 268-276.

Narasimhan, A., Jha, K. K., & Gopal, L. (2010). Transient simulations of heat transfer in human eye undergoing laser surgery. International Journal of Heat and Mass Transfer, 53(1), 482-490.

WHO. Vision 2020: right to sight. Blindness and visual impairment: global facts. (2007). at <http://www.who.int/blindness/Vision2020_report.pdf>. Accessed: April 28 2014

White, T. J., Mainster, M. A., Tips, J. H., & Wilson, P. W. (1970). Chorioretinal thermal behavior. *The Bulletin of mathematical biophysics*, *32*(3), 315-322.

Zhang R, Verkruysse W, Aguilar G, Nelson JS. 2005. Comparison of diffusion approximation and Monte Carlo based finite element models for simulating thermal responses to laser irradiation in discrete vessels. Physics in Medicine and Biology, 50 (17): 4075-4086.

Zhu, L., Banerjee, R. K., Salloum, M., Flower, R. W., & Bachmann, A. (2008). "Temperature Distribution During ICG-Dye-Enhanced Laser Photocoagulation of Feeder Vessels in Treatment of AMD-Related Choroidal Neovascularization," *Journal of biomechanical engineering*, 130(3), 031010.